www.cadanda.com Computer-Aided Design AND APPLICATIONS

Vibration Study of Novel Compliant Needle used for Vibration-assisted Needle Insertion

Yi Cai[1], Jason Moore[2] and Yuan-Shin Lee[3]

[1]North Carolina Agricultural and Technical State University, ycai@ncat.edu
[2]Pennsylvania State University, jzm14@psu.edu
[3]North Carolina State University, yslee@ncsu.edu

Corresponding author: Yi Cai, ycai@ncat.edu

ABSTRACT

Needles are among the most widely used medical devices, and their placement accuracy significantly affects the effectiveness of a treatment and the success or precision of a diagnosis. Vibration-assisted needle insertion is a dynamic insertion technique which can improve needle insertion accuracy by reducing the insertion force. This paper presents the vibration analysis of a novel compliant needle design for vibration-assisted insertion in medical applications. The needle design is featured by its 4-bevel needle tip and micro-slots on the needle shaft. Harmonic analysis was applied to reveal the relationship between slot location and transverse vibration amplitude, and an empirical method was developed to determine the slot locations which lead to maximum and minimum transverse amplitudes. The results were evaluated and validated by actual amplitude measurement of selected needle prototypes. Insertion experiment into tissue phantom was then conducted using these prototypes to investigate how transverse vibration amplitude affect insertion force. It was found that adding transverses vibration of small amplitude to axial vibration had the best outcome. This paper provides useful practical guidelines for design and optimization of needles for vibration-assisted insertion in medical applications and for improvement of insertion accuracy.

Keywords: vibratory needle insertion, vibration analysis, biomedical applications.
DOI: https://doi.org/10.14733.2019.742-754

1 INTRODUCTION

Needles are among the most widely used medical devices, and they serve in a wide variety of percutaneous procedures, from ordinary ones like blood sampling, regional anesthesia and drug delivery to complicated ones like tissue biopsy and brachytherapy [3]. The effectiveness of a treatment and the success or precision of a diagnosis is highly dependent on the accuracy of percutaneous insertion [12]. In procedures such as biopsy (for prostate, kidney, breast and liver), brachytherapy and anesthetic, placement accuracy of millimeters is required while in brain, fetus, eye and ear procedures placement accuracy of sub-millimeter is desirable. Furthermore, the target might be in the millimeter neighborhood of another organ, vessel or nerve. Therefore, extra caution is required to avoid any damage or spread of a disease which in turn may lead to subsequent complications.

Clinical studies have revealed that common factors that contribute to needle misplacement in percutaneous procedures include human errors [20], imaging limitations [3], target uncertainty [11], tissue deformation and needle deflection [1, 2]. Among these factors, tissue deformation and needle bending are directly related to the forces experienced by the needle during the insertion procedure in a proportional manner [25]. Accordingly, a practical approach to reduce needle placement errors is to reduce the insertion force [15]. Low insertion force also results in less pain, trauma and edema to the patients, which increases procedures efficacy and allows for shorter recovery time [4, 18].

According to DiMaio and Salcudean [12, 13], the insertion force comprised of two major components: a uniform axial friction force between the needle and the tissue along the shaft, and a force peak of cutting at the needle tip. To date, researchers have explored a variety of methods to reduce the insertion force. Modeling, optimization and innovation of needle geometries (rake angle, inclination angle, diameter, etc.) were conducted to reduce the tip force [22, 26], while special treatments of needle surface [14, 25] were demonstrated to be helpful for reducing the friction. Some researchers also tried to optimize insertion process via velocity control and trajectory selection, etc. [5, 17, 27].

Among all these methods, vibration-assisted needle insertion is a dynamic insertion technique where low-amplitude high-frequency vibration is applied to a needle in addition to the main insertion motion. It has been demonstrated by researchers that it not only reduces the tissue cutting force at the needle tip, but also reduces the friction between needle shaft and tissue under certain conditions [7, 16, 17, 19, 24]. A common limitation in the above research is that the dynamics of the vibrating needles was not studied, or at least not systematically. As a result, there is no guarantee has the applied vibration frequency has the best match with the needle. For example, the needle may have a length that can result in limited vibration amplitude at the tip under the applied frequency. Although sometimes the vibration amplitude at the needle tip were measured using optical or other methods, it seems not be able to provide direct guidance on how to fine-tune the amplitude if needed by the application requirements, given the limited number of tested needles. A systematic study is therefore needed for the dynamics of the needle vibration, so that the tip vibration mode of a needle can be determined, controlled and fine-tuned to optimal for different insertion situations, e.g. insertion into muscle tissue and skin. Another limitation is that only needles with ordinary tip geometries were tested and only axial or transverse vibration was applied. It still remains to be seen whether new needle tip design exists to better take advantage of vibration and whether a combination of axial and transverse vibration can further benefit. The potentials of vibratory insertion have not yet been fully explored in terms of needle geometry and vibration mode.

This paper aims at investigating two questions: (1) how geometric design parameters of a needle affect the vibration mode at the needle tip and (2) how the vibration mode at the needle tip affects the insertion performance in terms of insertion force. For the first question, harmonic analysis based on finite element analysis is used upon needles with different geometric design parameters, and an empirical method is proposed to improve the search efficiency of maximum and minimum transverse amplitudes. For the second question, vibration-assisted insertion experiment into tissue phantom is conducted using needle prototypes with different tip vibration modes.

2 NOVEL COMPLIANT NEEDLE FOR VIBRATION-ASSISTED INSERTION

In the earlier work of the authors presented in [9], an new needle geometric design for vibration-assisted needles were developed for medical treatments. Fig. 1(a) shows the design of the medical needle for vibratory insertion. The needle tip is featured by the 4 bevels forming the needle tip and a micro slot on the shaft. The bevels are symmetrically distributed to form a spear shape.

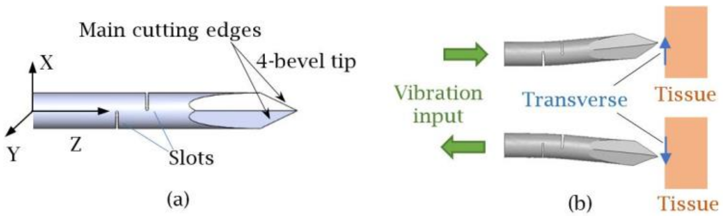

Figure 1: The proposed needle design: (a) overview and (b) illustrative insertion.

Among the four edges formed by the four bevels, the two associated the sharp corners of the spear shape are the main cutting edges during needle insertion. The micro slot, where lies the major novelty of the proposed design, aims at modifying the stiffness symmetry of the needle and thus the frequency response. The slot is cut along the X axis direction, so the main cutting edges is to vibrate more easily along X direction than Y direction. This design enables the main cutting edges to vibrate with high speed along both the Z and the X direction under axial stimulation at the base to perform micro tissue cutting, which will be beneficial to reduce the axial insertion force. An illustrative picture is shown in Fig. 1(b). The slot parameters include the number of slots, slot locations, depths and widths. It should be pointed out that the proposed needle is solid, so it can’t be used like common hollow percutaneous needles for syringe injection. Instead, it will be used as the stylet section of the stylet/cannula combination widely used in biopsy and brachytherapy needles and trocars.

Needle prototypes of the proposed design were fabricated using micro-EDM with different slot parameters, and they were used to conduct several different experiments. When a piezoelectric actuator with a highest frequency of 1500 Hz was used, the insertion force tended to be even higher than when no vibration was applied [8]. However, when an ultrasonic vibrator with a working frequency of 20 kHz was used, the insertion force could be significantly lower than when no vibration or only axial vibration was applied, depending on the location of slots and the resultant tip vibration modes [9].

The preliminary results showed the potentials of the proposed design, and indicated the necessity for more experiments. Meanwhile, a systematic study of needle vibration dynamics is needed to find out the tip vibration mode of a needle with specific slot parameters under given vibration parameters. It will help to identify slot parameters which result in tip vibration modes to be tested in future insertion experiments, instead of testing needles with randomly assigned slot parameters. For example, it is possible to prepare a set of needles with similar axial vibration amplitudes but increasing transverse amplitudes by manipulating the slot parameters, so that the effect of transverse vibration can be clearly studied and the experiment is in a more controlled manner. As can be imagined, the optimal tip vibration mode for insertion into soft tissue is likely to be different from that into tough tissue like skin. A study of vibration dynamics can also determine the corresponding slot parameters if a specific tip vibration mode is needed for the given application. A dynamics study of the vibrating compliant needles based on harmonic analysis is therefore presented in the next section.

3 VIBRATION ANALYSIS OF COMPLIANT NEEDLES

3.1 Harmonic Analysis

Fig. 2 shows the schematic of the ultrasonic vibration-assisted insertion device, which is adapted from typical ultrasonic welding machines. The boundary conditions of the needle are modeled as free–free where each end of the needle is free to move. Other researchers have also used free–free boundary conditions in modeling ultrasonic machining tools [23].

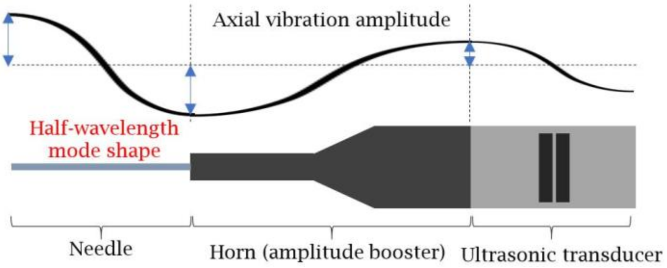

Figure 2: Amplitude chain of axial vibration in ultrasonic insertion device.

For a homogeneous rod subjected to free vibration, the system is considered as a continuous system in which the beam mass is distributed along with the stiffness of the shaft. The equation of longitudinal wave propagation can be written as [21]

$$-\frac{d}{dx}\left[EA(x)\frac{dU(x)}{dx}\right] = \omega_a^2 \rho A(x) U(x) \tag{3.1}$$

where *E* is the Young's modulus of the material, *A(x)* is the cross-sectional area of the needle at a given position *x* from the base, ρ is the density of the needle material, ω_a is the axial resonant frequency of the needle, and *U(x)* is the axial displacement of the needle at a given position *x*. The corresponding boundary conditions for Eqn. (3.1) are $U'(0) = 0$ and $U'(L) = 0$, where L is the length of needle. When the excitation frequency has been determined by the device, the needle length can be calculated as

$$L = \frac{i}{2f_{excitation}}\sqrt{\frac{E}{\rho}} \quad (i = 1, 2, \cdots) \tag{3.2}$$

Fig. 2 refers to the situation *i* = 1, where the needle length equals half of the wavelength of wave propagation in the needle [9]. This mode shape generates the maximum amplitude of axial vibration at the ends of the needle. With a Young's Module *E* = 190 GPa and a density of ρ = 8000 kg/m^3 for AISI 304 stainless steel, L was calculated as 60.9 *mm* for an excitation frequency of $f_{excitation} = 40$ kHz.

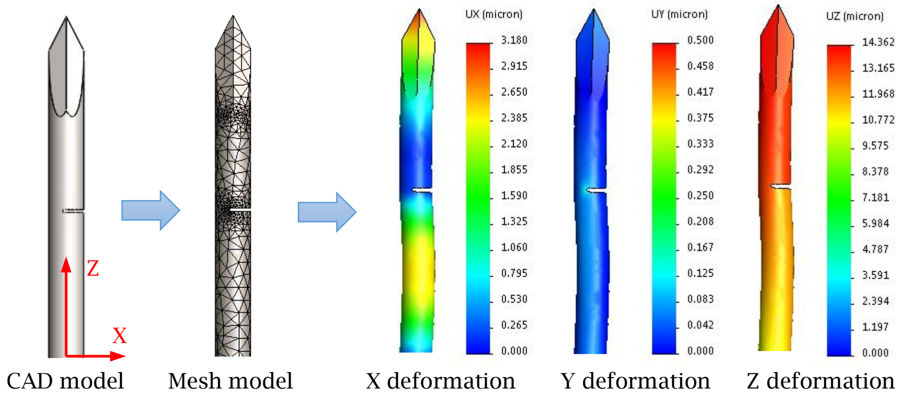

Figure 3: Harmonic analysis of the compliant needles.

To study the effects of shaft slots on vibration modes, we began with the situation of one slot. According to the earlier work of the authors [10], slot width had limited influence on tip vibration amplitude, while slot depth had a great impact on tip vibration but also on needle strength. Moreover, the slot depth was difficult to precisely control due to the small slot size and circular cross-session of the needle. Out of the considerations of needle strength and ease of control during needle fabrication, slot location is focused on in this paper. The CAD models of 13 needles, namely N4 to N16, with one slot were built in SolidWorks where the distance between the tip and the slot changed from 4 *mm* to 16 *mm* with an interval of 1 *mm*. The results of needles with larger slot-tip distances were not listed because transverse vibration was only needed at the region close to needle tip, and a slot distant from the tip will increase the tendency of needle buckling. The slot width W was 100 μm, and the slot depth was 0.6D, where D was the needle diameter being 1.27 *mm* (Gauge 18). For meshing of CAD models, the maximum element size was set to be 0.5 *mm*, the minimum was 0.05 *mm*. The minimum number of elements in a circle was 8, and the element size growth ratio was 1.5. The resultant number of nodes was 23987, and the number of elements was 14719. The maximum Jacobian Ratio was 3.47, the maximum aspect ratio of the elements was 4.43, and 99.5% of the elements had an aspect ratio lower than 3. All these parameters were under suitable ranges. Harmonic analysis was conducted to individual needle using an axial excitement with a peak-peak amplitude of 12.5 μm applied at the bottom of each needle between the frequencies of 38 kHz and 42 kHz. This amplitude range was based on the capability of the available vibration device. As illustration, the deformation results of N7 as its displacements in the three directions at 40 kHz can be seen in Fig. 3.

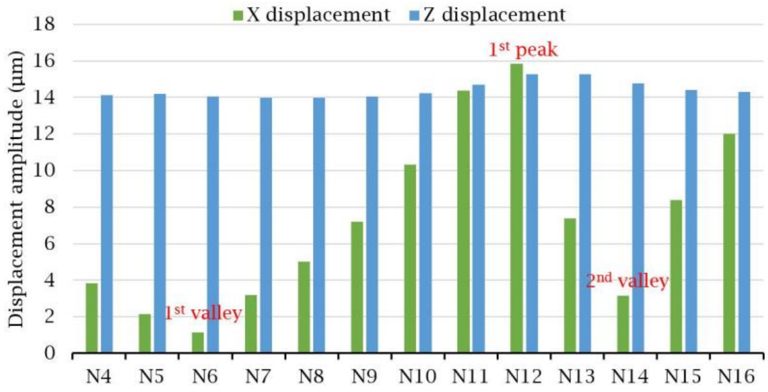

Figure 4: Results of simulated X and Z displacement for N4 to N16 at 40 kHz.

For all the 13 needles, the X (transverse) and Z (axial) direction displacement of the needle tip were recorded. The displacement in the Y direction was at the magnitude of 10^{-1} μm and thus not recorded. Fig. 4 shows the results of X and Z displacement at the needle tip of N4 to N16 at 40 kHz. The Z displacements stay slightly higher than the excitation amplitude of 12.5 μm among all the needles. This should be because the slot enabled the front section of a needle to perform more movement in the axial direction. It is interesting to notice that the X displacement changes in a period-like manner as the slot location changed from 4 *mm* to 16 *mm*. It reaches the peak value of 15.86 μm in N12, and valley values in N6 and N14. It is anticipated that another peak will appear after N16. It should be noticed that the peak value does not occur in the exact middle of two valleys, i.e. somewhere near N10. The harmonic analysis also provided stress information on the needles. It was found that the maximum stress on a needle occurred at the bottom of the slot, and a larger transverse displacement at the needle tip was associated with a larger value of maximum stress. Accordingly, N12 had the largest value of maximum stress among all the needles which was 166 MPa. Although this was below the yield strength of 304 stainless steel which is 215 MPa, fatigue analysis and optimization should be conducted in the future due to the cyclic loading.

3.2 An Empirical Method for Amplitude Prediction

While harmonic analysis provides a useful method to find out the relationship between the slot location and the resultant transverse and axial vibration amplitude, it will be desirable to directly predict when a peak or valley value of X amplitude will occur without conducting harmonic analysis in a trial-and-error manner. In this section, an empirical method using equations from vibration theories is developed based on the observation of the mode shapes when a peak or valley value of X amplitude will occur.

For a cantilever beam subjected to free vibration, the equation of transverse motion can be written as [21]

$$\frac{d^2}{dx^2}\left[EI(x)\frac{d^2Y(x)}{dx^2}\right] = \omega_t^2\rho A(x)Y(x) \tag{3.3}$$

where *E* is the Young's modulus of the material, *I(x)* is the area moment of inertia of the needle cross section at a given position *x*, *A(x)* is the cross-sectional area of the needle at a given position *x*, ρ is the density of the needle material, ω_t is the transverse resonant frequency of the needle, and *Y(x)* is the transverse displacement of the needle at a given position *x*. *I(x)* is given as $\pi d^4/64$, where *d* is the diameter of the needle. With the setup shown in Fig. 2, since the diameter of the horn is significantly larger than that of the needle, the needle can be considered fixed at the base and free to move at the end like a cantilever beam. The corresponding fixed-free boundary conditions for Eqn. (3.3) are $Y(0) = 0$, $Y'(0) = 0$, $Y''(L) = 0$ and $Y'''(L) = 0$. By solving this equation numerically, the transverse resonant frequencies are given as

$$f_{fixed-free(i)} = \frac{(\beta_i L)^2}{2\pi}\sqrt{\frac{EI}{\rho S L^4}} \quad \left(\beta_1 L = 1.875, \beta_2 L = 4.694, \beta_3 L = 7.855, \beta_i L \approx \frac{2i-1}{2}\pi, i \geq 4\right) \tag{3.4}$$

If a needle is fixed at one end and simply supported at the other end, the corresponding fixed-simple boundary conditions for Eqn. (3.3) are $Y(0) = 0$, $Y'(0) = 0$, $Y(L) = 0$ and $Y''(L) = 0$. The transverse resonant frequencies are given as

$$f_{fixed-simple(i)} = \frac{(\beta_i L)^2}{2\pi}\sqrt{\frac{EI}{\rho S L^4}} \quad \left(\beta_1 L = 3.927, \beta_2 L = 7.069, \beta_3 L = 10.210, \beta_i L \approx \frac{4i+1}{4}\pi, i \geq 4\right) \tag{3.5}$$

To find out how the X displacement changes along with the slot location, the mode shape of N12 at 40 kHz is presented in Fig. 5(a), where the first peak value occurs as the slot location changes. It is observed that the needle can be divided into two sections in this mode shape. The section between the needle tip and the slot is in the rigid body mode which does not deform, while the section between the needle base and the slot is close to the 7th transverse bending mode under fixed-free boundary condition. By making $f_{excitation}$ = 40 kHz and *i* =7 in Eqn. (3.4), it is found the corresponding needle length at resonance is 50.7 *mm*. This matches the distance between the needle base and the slot in N12 used in harmonic analysis, which is 48.9 *mm* by subtracting 12 *mm* from 60.9 *mm*. The peak value in N12 can be considered to mainly result from the large deformation at the end of the base section under fixed-free transverse vibration resonance.

To find out when valley values occur, the mode shape of N6 at 40 kHz is presented in Fig. 5(b). It is found that the needle can also be divided into two sections in this mode shape. The section between the needle tip and the slot is in the rigid body mode which does not deform, while the section between the needle base and the slot is close to the 7th transverse bending mode under fixed-simple boundary condition. By making $f_{excitation}$ = 40 kHz and *i* = 7 in Eqn. (3.5) it is found the corresponding needle length at resonance is 56.5 *mm*. This matches the distance between the needle base and the slot in N6, which is 54.9 *mm*. The valley value in N6 can be considered to mainly result from the small deformation at the end of the base section under fixed-simple transverse vibration resonance. Similarly, by making $f_{excitation}$ = 40 kHz and *i* = 6 in Eqn. (3.5), it is found the corresponding needle length at resonance is 48.6 *mm*. This matches the distance between the needle base and the slot in

N14, which is 46.9 *mm*. Fig. 5(c) shows the mode shape of N14 at 40 kHz. The base section is close to the 6th transverse bending mode under fixed-simple boundary condition as predicted.

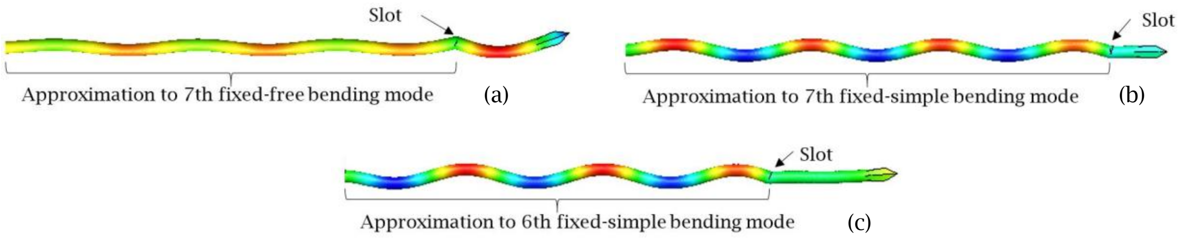

Figure 5: Needle mode shapes at 40 kHz: (a) N12, (b) N6 and (c) N14.

The above method can be implemented more conveniently with Fig. 6, which shows the relationship between resonant length and resonant frequency under free-free axial vibration and fixed-free transverse bending vibration. The red dotted curve on the upper right is based on Eqn. (3.2) when *i* = 1, while other continuous curves are based on Eqn. (3.4) when *i* changes from 1 to 12. For example, if the working frequency is 40 kHz, by drawing a horizontal line and make it intersect with the red dotted curve, the needle length can be obtained as 60.9 *mm* (Point A). The same horizontal line also intersects with the 7th transverse curve at the length of 50.7 *mm* (Point B). According to the proposed empirical method, the first peak in X displacement will occur when the distance between the needle tip and slot is around 10.2 *mm* by subtracting 50.7 *mm* from 60.9 *mm*. This distance corresponds to somewhere between N10 and N11 and close to N12.

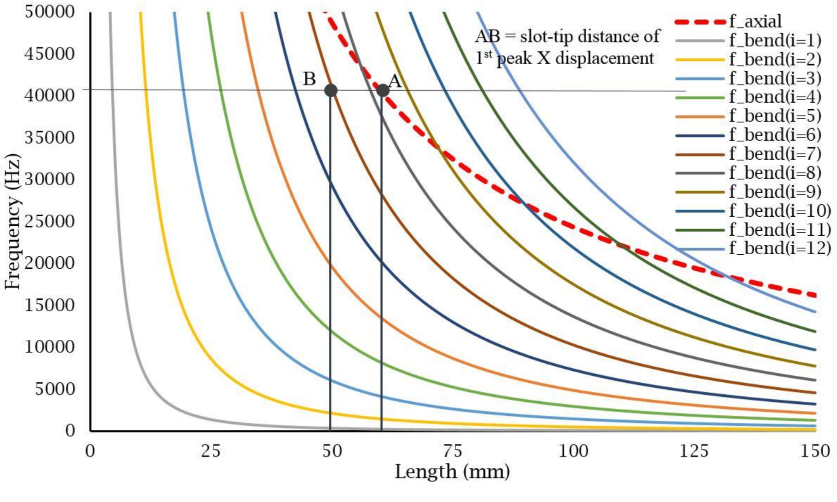

Figure 6: Relationship between resonant length and resonant frequency for different vibration conditions.

	20 kHz				40 kHz		
Needle length	121.8 *mm*				60.9 *mm*		
Location	1st peak	1st valley	2nd peak	2nd valley	1st valley	1st peak	2nd valley

Calculated slot-base distance	115.7 *mm*	112.7 *mm*	104.7 *mm*	101.8 *mm*	56.5 *mm*	50.7 *mm*	48.6 *mm*
Simulated slot-base distance	114.8 *mm*	111.8 *mm*	103.8 *mm*	100.8 *mm*	54.9 *mm*	48.9 *mm*	46.9 *mm*
Relative error	0.78%	0.81%	0.87%	0.99%	2.91%	3.68%	3.62%

Table 1: Summary of the calculated and simulated slot-base distance at peaks and valleys.

The empirical method presented above provides a convenient way to estimate the corresponding distance between the needle base and the slot when peak and valley X displacements occur. Tab. 1 summaries the results for both 20 kHz and 40 kHz situations with 1 *mm* slot location intervals. It can be seen that as the needle length in 40 kHz becomes only half of that in 20 kHz, the relative error increases as a shorter needle tends to be more sensitive to the location of the slot. The minor difference between the calculated and simulated values results from the fact that the equations are developed for rods with constant cross-section while the needle tip is not. This makes the calculated distances always greater than the simulated ones. Another source of inaccuracy comes from the approximation of the status at the slot location. When calculating the distance for peak X displacements, the slot was approximated as a free end, while for valley X displacements, it was as a simply supported end. Actually, due to the front section of the needle, the slot location can't be entirely free or rotate as simply supported. The accuracy of the method will be further validated and evaluated in next section with microscopic measurement of vibration amplitude for needle prototypes used in insertion experiments.

4 VIBRATORY INSERTION EXPERIMENT

4.1 Measurement of Vibration Amplitude

To study the effects of needle tip vibration modes on insertion performance, four needle prototypes with one slot, together with a control needle without slots, were fabricated using micro-EDM [10] with the dimensions shown in Tab. 2. The four needles with slot were chosen based on Fig. 4, where the X displacement at the needle tip increases from N6 to N12 and then decreases in N14 under 40 kHz excitation. They not only serve the purpose of insertion experiments, but also help to validate and evaluate the results of harmonic analysis and empirical method presented earlier in Section 3.

Needle	Length	φ	β	Diameter (D)	Slot-tip distance	Slot depth
N0(Control)	60.9 *mm*	10°	20°	1.27 *mm*	No slots	0.6D
N6					6 *mm*	
N9					9 *mm*	
N12					12 *mm*	
N14					14 *mm*	

Table 2: Summary of tested needle prototypes.

To determine the effects of the compliant geometry on the tip motion of the needles and thus evaluate the results in Section 3, the displacements of the tips were measured using a Hirox KH-7700 Advanced 3D Digital Microscope. Images with a resolution of 1600 × 1200 pixels were captured for each needle with and without vibration applied. The motion of the tip was determined by the long-exposure "ghost images" [6]. Fig. 7(a) shows the needle tip of N12 without applied vibration, where the light-reflecting spots on surface textures are clear and sharp. Fig. 7(b) shows the same needle tip with applied vibration, where the light-reflecting spots become fuzzy areas. The displacement can be obtained by subtracting the size of the light-reflecting spots without applied vibration from the size of the fuzzy areas of the spots with applied vibration. The exposure time for the images was 8 *ms*. At 40 kHz frequency, this allowed for 320 cycles to be captured in each image, ensuring the capture of the full range of motion. The motion was recorded for the output end of the horn and each of the five needles used in this study.

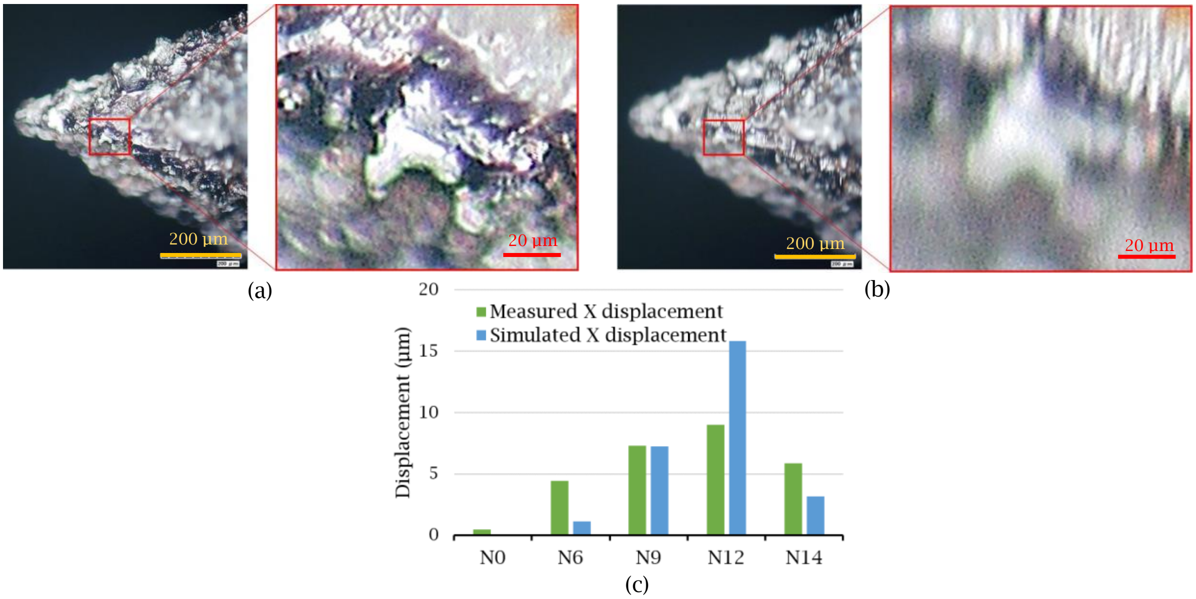

Figure 7: Measurement of vibration amplitude using microscopic images: (a) without applied vibration, (b) with applied vibration, and (c) comparison with simulated results.

The results of measured X displacements are shown in Fig. 7(c) together with the simulated results from harmonic analysis extracted from earlier Fig. 4. The peak-peak motion amplitude at the end of the horn was 12.5 μm. Ideally, the control needle N0 should only have motion in the axial direction of the vibration. However, minor transverse vibration motion was still observed, which may be due to needle fabrication asymmetry and environment disturbance. The needles with slot had motion in both the axial direction and the transverse direction. As the distance between the tip and slot increases from N6 to N12, the transverse displacement also increases, followed by a drop in N14. This follows the overall trend of the results of harmonic analysis in Fig. 4. The measured amplitudes are not exactly the same with those in simulation, which should be due to the difference between the Young's modulus and density of the actual needles and those used in simulation, as well as the damping in the actual system.

4.2 Insertion Experiment

Fig. 8(a) shows the setup for the tissue phantom experiment. A linear motion guide was utilized to insert the needle into tissue phantom at a constant rate. It was controlled by an Arduino Mega 2560 microcontroller and a TB6600 stepper motor driver. A 50W 40 kHz ultrasonic transducer together with a horn was mounted to the slide on the linear motor to provide vibration during the tests. A strain gauge load cell (Lotoclub) of a capacity of 30 N was used to measure the force along the insertion direction, and it was attached to a support structure fixed on an adjacent table for vibration isolation. A 9V DC voltage was supplied to the strain gauge load cell, and an INA 125 instrumentation amplifier was used to amplify the gauge output with a gain of 604. A data acquisition system (National

Instruments, USB-6002) and LabVIEW software were used to record the force data. A polyurethane sheet (M-F Manufacturing) with a Shore Hardness of 40A and a thickness of 1.588 *mm* was used here as an analog to human skin. A rotational structure was used to hold the testing medium which was clamped by two plates with screws. The plates had 12 aligned holes in them. By rotating the plates together with the phantom, a needle can pass through the phantom at 12 different locations.

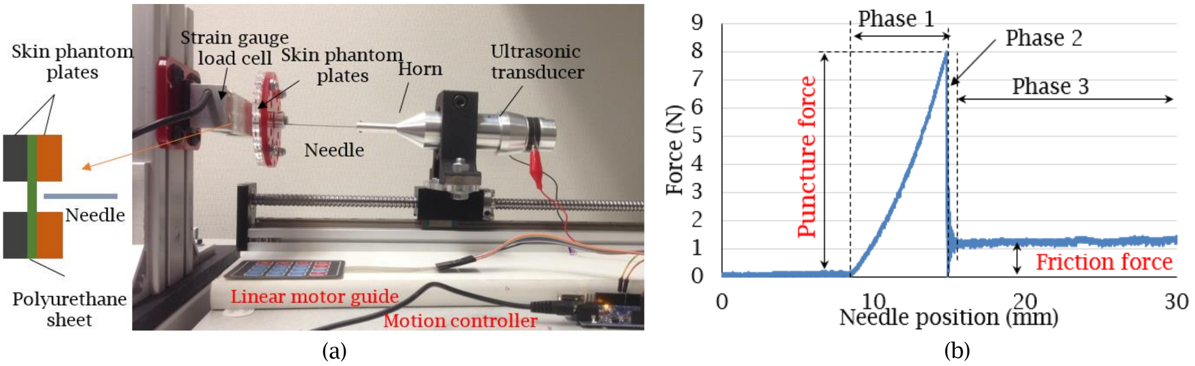

Figure 8: Vibratory insertion experiment: (a) experiment setup and (b) example force-position plot.

The five needles in Tab.2 were used in this study. The control needle N0 was inserted with and without applied vibration, while each of the other four needles with slots was inserted with an applied axial ultrasonic vibration of 40 kHz, resulting in six needle-vibration combinations. Five trials were conducted for each combination. The average velocity of insertion was set to a constant of 2 *mm/s* for all the trials, and the force data were collected for each trial with a sampling rate of 1000 Hz. An example force-position plot is shown in Fig 8(b), where three phases can be identified during the insertion process. In the first phase, the needle tip touches the skin phantom but no cutting or penetration occurs. The force is mainly caused by the elastic deformation of the skin phantom. In the second phase, the needle tip quickly cuts and punctures through the skin phantom, which is featured by a significant drop in the force. Since the deformation happened in a short time, the force fluctuates due to the elastic property of the load cell. In the third phase, the needle tip has exited the phantom skin. The force is mainly caused by the friction between the needle shaft and the inner surface of puncture hole. Two parameters were measured as needle performance indicators. The first parameter is the puncture force, which is the peak value of insertion force before it suddenly drops. It is the maximum force the phantom endures before penetration begins. The second parameter is the friction force in the third phase. Keeping these two parameters low is usually preferred.

The results are shown in Fig. 9(a) and 9(b), respectively. Compared to the control insertion with no vibration, the puncture force was reduced with applied vibration by 4.98% for the control needle N0, and by 7.21% and 16.75% for N6 and N14, respectively. The ANOVA F-test p-values were 0.001, 0.001 and 0.001 respectively. On the other hand, the puncture force was increased by 4.36% and 8.09% for N9 and N12, respectively. The ANOVA F-test p-values were 0.013 and 0.010, respectively. N14 had the lowest mean value of puncture force, and it was tested to be significantly lower than the puncture forces of other needles. The friction force was reduced with applied vibration by 2.16%, 17.83%, 27.43% and 25.29% for N0, N9, N12 to N14, respectively. The ANOVA F-test p-values were 0.778, 0.060, 0.001 and 0.005, respectively. On the other hand, the friction force was increased by 8.58% for N6 with the ANOVA F-test p-value of 0.123. Although N12 had the lowest mean value of friction force, it was not significantly lower than that of N9 and N14 with ANOVA F-test p-values of 0.234 and 0.728, respectively.

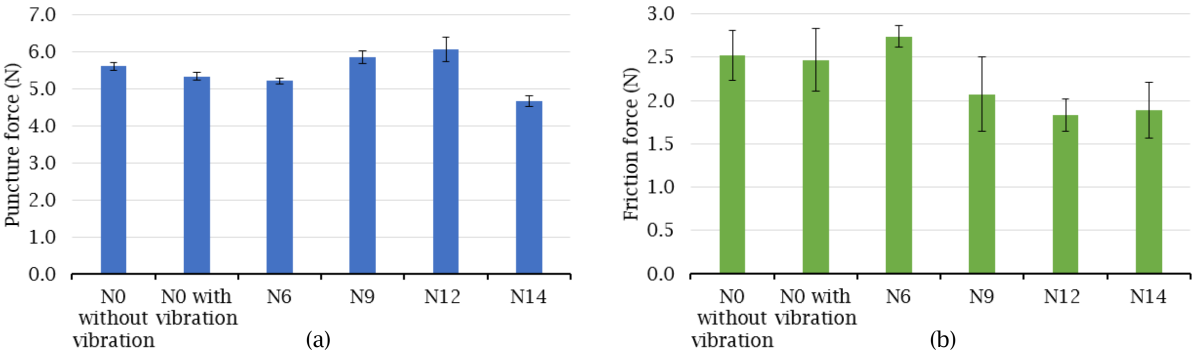

Figure 9: Experiment results: (a) puncture force and (b) friction force.

By relating Fig. 9 and Fig. 7, it seems that a small amplitude of transverse vibration was helpful to further reduce the puncture force. As the amplitude increased, since the polyurethane film was relatively tough, the cutting edges of the needle were not able to cut a larger incision opening directly as expected with just a few microns of transverse vibration. Instead, the increased transverse motion increased the transverse compressive force applied on the needle tip area, resulting higher resistant force. Moreover, the needle tip was not interacting with the testing medium with its best perpendicular orientation. Both of these would increase the puncture force, so some needles like N9 and N12 even had larger puncture force with applied vibration than N0 without applied vibration. As the polyurethane film was finally penetrated with a larger puncture force, a larger area around the needle tip was affected and a larger incision crack was formed. This explained why the needles with larger puncture forces tended to have lower friction forces, just like the four needles with slots.

The above analysis can be supported by measuring the incision cracks on the polyurethane sheet after the insertion experiment using microscopic camera. Fig. 10(a) and 10(b) shows two examples of the cracks, which were formed by N9 and N12, respectively. Fig. 10(c) shows the results of crack length of the needles. As predicted, a larger crack is associated with larger puncture force and lower friction force. It is also noticed that the standard deviation of N12 is much greater than other needles, indicating the formation of large cracks may be unstable.

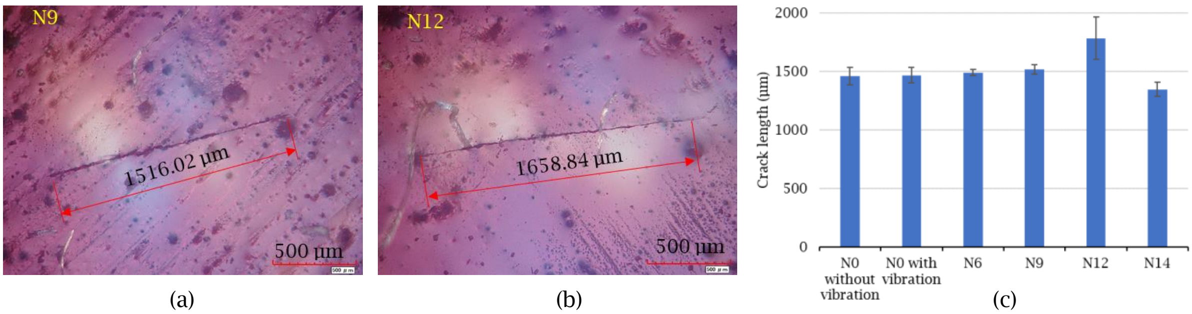

Figure 10: Cracks formed by needles on the polyurethane sheet: (a) N9, (b) N12 and (c) comparison of crack lengths.

5 CONCLUSIONS

This paper presented the vibration study of a design of novel compliant needle proposed for vibration-assisted insertion in medical applications. Harmonic analysis was conducted to study how the slot parameters affect the vibration mode at the needle tip. The results of harmonic analysis revealed that the transverse vibration amplitude changed in a periodic manner as the slot moved away from the tip, resulting several local amplitude peaks and valleys to choose from for different applications. An empirical method was then developed to determine the slot locations which lead to maximum and minimum transverse amplitudes. The accuracy of the harmonic analysis and empirical method were evaluated and validated by actual amplitude measurement of selected needle prototypes. Vibration-assisted insertion experiment into polyurethane sheets was conducted to study the effects of needle tip vibration modes on insertion performance. The results of insertion experiment showed that axial vibration together with a proper level of transverse vibration (6 μm in this case) gave the best effect in force reduction for the tested polyurethane material which mimicked human skin. This paper provides useful practical guidelines for design and optimization of needles for vibration-assisted insertion in medical applications, and for improvement of insertion accuracy.

ACKNOWLEDGEMENTS

This work was supported by the NSF Grants (CMMI-1125872, CMMI-1404916 and CMMI-1547105) to North Carolina State University and the NSF Grant (CMMI-1404916) to The Penn State University. Their support is highly appreciated.

Yi Cai, http://orcid.org/0000-0002-7587-8956
Jason Moore, http://orcid.org/0000-0002-8830-2833
Yuan-Shin Lee, http://orcid.org/0000-0001-9892-5199

REFERENCES

[1] Abolhassani, N.; Patel, R.; Ayazi, F.: Effects of different insertion methods on reducing needle deflection, Proceedings of the 29th IEEE Annual International Conference of EMBS, Lyon, France, 2007, 491-494. https://doi.org/10.1109/IEMBS.2007.4352330
[2] Abolhassani, N.; Patel, R.; Moallem, M.: Control of soft tissue deformation during robotic needle insertion, Minimally Invasive Therapy & Allied Technologies, 15(3), 2006, 165-176. https://doi.org/10.1080/13645700600771645
[3] Abolhassani, N.; Patel, R.; Moallem, M.: Needle insertion into soft tissue: A survey, Medical Engineering & Physics, 29(4), 2007, 413-431. https://doi.org/10.1016/j.medengphy.2006.07.003
[4] Abolhassani, N.; Patel, R. V.; Ayazi, F.: Minimization of needle deflection in robot-assisted percutaneous therapy, The International Journal of Medical Robotics and Computer Assisted Surgery, 3(2), 2007, 140-148. https://doi.org/10.1002/rcs.136
[5] Badaan, S.; Petrisor, D.; Kim, C.; Mozer, P.; Mazilu, D.; Gruionu, L.; Patriciu, A.; Cleary, K.; Stoianovici, D.: Does needle rotation improve lesion targeting?, The International Journal of Medical Robotics and Computer Assisted Surgery, 7(2), 2011, 138-147. https://doi.org/10.1002/rcs.381
[6] Barnett, A. C.; Jones, J. A.; Lee, Y.-S.; Moore, J. Z.: Compliant Needle Vibration Cutting of Soft Tissue, Journal of Manufacturing Science and Engineering, 138(11), 2016, 111011-111011. https://doi.org/10.1115/1.4033690
[7] Barnett, A. C.; Wolkowicz, K.; Moore, J. Z.: Vibrating Needle Cutting Force, Proceedings of ASME 2014 International Manufacturing Science and Engineering Conference, Ann Arbor, Michigan, USA, 2014, V002T02A025. https://doi.org/10.1115/MSEC2014-4049
[8] Cai, Y.; Moore, J.; Lee, Y.-S.: Intricate Geometric Design and Manufacturing on Vibration-assisted Needles for Medical Applications, Proceedings of ASME 2016 International Manufacturing Science and Engineering Conference, Virginia Tech, Blacksburg, VA, USA, 2016, V002T03A011-V002T03A011. https://doi.org/10.1115/MSEC2016-8743
[9] Cai, Y.; Moore, J.; Lee, Y.-S.: Novel Surgical Needle Design and Manufacturing for Vibration-assisted Insertion in Medical Applications, Computer-Aided Design and Applications, 14(6), 2017, 1-11. https://doi.org/10.1080/16864360.2017.1287759

[10] Cai, Y.; Moore, J.; Lee, Y.-S.: Thin-Slots Machining of Compliant Needles for Vibration-assisted Medical Insertion, Procedia Manufacturing*,* 10, 2017, 392-406. https://doi.org/10.1016/j.promfg.2017.07.012

[11] Carr, J. J.; Hemler, P. F.; Halford, P. W.; Freimanis, R. I.; Choplin, R. H.; Chen, M. Y.: Stereotactic Localization of Breast Lesions: How It Works and Methods to Improve Accuracy, Radiographics*,* 21(2), 2001, 463-473. https://doi.org/10.1148/radiographics.21.2.g01mr11463

[12] DiMaio, S. P.; Salcudean, S. E.: Needle insertion modeling and simulation, IEEE Transactions on Robotics and Automation*,* 19(5), 2003, 864-875. https://doi.org/10.1109/TRA.2003.817044

[13] DiMaio, S. P.; Salcudean, S. E.: Interactive simulation of needle insertion models, IEEE Transactions on Biomedical Engineering*,* 52(7), 2005, 1167-1179. https://doi.org/10.1109/tbme.2005.847548

[14] Doerzbacher, M.; Barnett, A.; Brandmeir, N.; Wolfe, D.; Zheng, S.; Moore, J.: Advanced Needle Coatings for Improved Lumbar Drain Procedure, Journal of Medical Devices*,* 7(3), 2013, 030942. https://doi.org/10.1115/1.4024485

[15] Han, P.; Kim, J.; Ehmann, K. F.; Cao, J.: Laser surface texturing of medical needles for friction control, International Journal of Mechatronics and Manufacturing Systems 1*,* 6(3), 2013, 215-228. https://doi.org/10.1504/IJMMS.2013.056449

[16] Huang, Y. C.; Tsai, M. C.; Lin, C. H.: A piezoelectric vibration-based syringe for reducing insertion force, IOP Conference Series: Materials Science and Engineering*,* 42(1), 2012, 012020. https://doi.org/10.1088/1757-899X/42/1/012020

[17] Kaiguo, Y.; Wan Sing, N.; Keck Voon, L.; Tien, I. L.; Yan, Y.; Podder, T.: High Frequency Translational Oscillation and Rotational Drilling of the Needle in Reducing Target Movement, Proceedings of IEEE International Symposium on CIRA Espoo, Finland, 2005, 163-168. https://doi.org/10.1109/cira.2005.1554271

[18] Karnopp, D.: Computer simulation of stick-slip friction in mechanical dynamic systems, Journal of dynamic systems, measurement, and control*,* 107(1), 1985, 100-103. https://doi.org/10.1115/1.3140698

[19] Khalaji, I.; Hadavand, M.; Asadian, A.; Patel, R. V.; Naish, M. D.: Analysis of needle-tissue friction during vibration-assisted needle insertion, Proceedings of IEEE/RSJ International Conference on Intelligent Robots and Systems (IROS), Tokyo, Japan, 2013, 4099-4104. https://doi.org/10.1109/IROS.2013.6696943

[20] Kohn, L. T.; Corrigan, J. M.; Donaldson, M. S., Eds., *To err is human: building a Safer Health System*. Washington DC, US: National Academies Press, 2000. https://doi.org/10.17226/9728

[21] Meirovitch, L., Analytical methods in vibration. The Mcmillan Company, New York, NY, 1967.

[22] Moore, J. Z.; McLaughlin, P. W.; Shih, A. J.: Novel needle cutting edge geometry for end-cut biopsy, Medical Physics*,* 39(1), 2012, 99-108. https://doi.org/10.1118/1.3665253

[23] Seah, K.; Wong, Y.; Lee, L.: Design of tool holders for ultrasonic machining using FEM, Journal of Materials Processing Technology*,* 37(1), 1993, 801-816. https://doi.org/10.1016/0924-0136(93)90138-V

[24] Shin-Ei, T.; Yuyama, K.; Ujihara, M.; Mabuchi, K.: Reduction of insertion force of medical devices into biological tissues by vibration, Japanese journal of medical electronics and biological Engineering*,* 39(4), 2001, 292-296. https://doi.org/10.11239/jsmbe1963.39.292

[25] Wang, X.; Han, P.; Kang, M.; Ehmann, K.: Surface-blended texturing of medical needles for friction reduction using a picosecond laser, Applied Physics A*,* 122(4), 2016, 1-9. https://doi.org/10.1007/s00339-016-9892-2

[26] Wang, Y.; Chen, R. K.; Tai, B. L.; Shih, A. J.: Advanced Five-Plane Lancet Needle Design, Grinding, and Tissue Insertion, Proceedings of ASME 2014 International Manufacturing Science and Engineering Conference, Detroit, Michigan, USA, 2014, V002T02A028. https://doi.org/10.1115/msec2014-4046

[27] Wolkowicz, K.; Moore, J. Z.; McLaughlin, P.: Novel Pneumatic Device for High Speed Needle Insertion in Brachytherapy, Journal of Medical Devices*,* 7(3), 2013, 030945-030945. https://doi.org/10.1115/1.4024513